Spectrochimica Acta Part A 82 (2011) 521–526

Contents lists available at ScienceDirect

Spectrochimica Acta Part A: Molecular and Biomolecular Spectroscopy

journal homepage: www.elsevier.com/locate/saa

Growth and characterization of 2-amino-4-picolinium toluene sulfonate single crystal

G. Anandha Babu*, P. Ramasamy

Centre for Crystal Growth, SSN College of Engineering, SSN Nagar, Kalavakkam 603 110, Tamilnadu, India

ARTICLE INFO

Article history:
Received 11 June 2011
Received in revised form 25 July 2011
Accepted 7 August 2011

PACS:
61.66.Hq
42.70.Nq
81.10.Dn
61.10.–i

Keywords:
Optical materials
Organic compounds
Crystal growth
Crystal structure
Defects

ABSTRACT

2-Amino-4-picolinium toluene sulfonate (2A4PTS), a new organic material, was synthesized and grown as single crystals in room temperature by slow evaporation solution growth technique using water as solvent. The crystal structure of 2A4PTS has been determined using single crystal X-ray diffraction studies. 2A4PTS belongs to monoclinic crystal system. The molecular arrangements in the crystal were studied. The structural perfection of the grown crystals has been analysed by high-resolution X-ray diffraction (HRXRD) rocking curve measurements. Fourier transform infrared (FTIR) spectral studies have been performed to identify the functional groups. The optical transmittance window and the lower cutoff wavelength of the 2A4PTS have been identified by UV–Vis–NIR studies. The nonlinear optical properties have been investigated by Z-scan method. The nonlinear refractive index and linear absorption coefficient of the 2A4PTS are found to be in the order of 10^{-8} cm^2/W and 10^{-4} cm/W, respectively. The laser induced surface damage threshold for the grown crystal was measured using Nd:YAG laser. Thermal analysis carried out on the compound reveals that 2A4PTS is stable up to 133 °C. The microhardness test was carried out and the load dependent hardness was measured.

1. Introduction

The origins of the nonlinear processes are well understood and the progress now depends on the development of materials technology compatible with the various device embodiments [1]. Compared to the extensive amount of research conducted on the synthesis and characterization of new molecular structures for second-order nonlinear optical applications, the study of third-order nonlinear processes on molecular materials has received relatively limited attention. Recently, the scope for the synthesis and characterization of third-order materials has expanded considerably. The impetus for this increased activity has been a quest for fundamental understanding of the structure property relationship and the strong technological interest in all optical signal processing provided by the third-order processes [2]. Development of novel molecular and crystal design techniques for assembling such materials is of great current interest [3,4]. The desirable properties of 2A4PTS which include stable physio-chemical properties and absence of any phase transition highlight this material as a potential candidate for nonlinear optical applications, and thereby attracted our interests towards a thorough investigation of this compound. In this paper, we report on synthesis, crystal growth, single crystal structure determination by single-crystal X-ray diffraction, high resolution X-ray diffraction, optical, thermal, laser-induced surface damage threshold, NLO properties by Z-scan technique and mechanical properties of 2A4PTS presented for the first time.

2. Material synthesis and single crystal growth

The 2A4PTS salt was obtained by dissolving 2 Amino 4-Picoline and p-Toluene sulfonic acid in methanol at room temperature in the molar ratio 1:1. The reaction scheme and the chemical structures are illustrated in Fig. 1. The salt was purified by the recrystallization process. The single crystals were grown from aqueous solution. Single crystal of size $15 \times 8 \times 5$ mm^3 has been obtained after a typical period of 90 days. Grown single crystals of 2A4PTS are shown in Fig. 2. As highlighted by the chemical bonding theory of single crystal growth, the growth shape of 2A4PTS single crystals is closely correlated to their crystallographic characteristics [5–10].

3. Sample characterization

3.1. Single-crystal X-ray diffraction study

The crystal structure was determined from the single crystal X-ray diffraction data obtained with a three-circle Enraf Nonius

* Corresponding author. Tel.: +91 4427475166; fax: +91 4427475166.
E-mail address: anandcgc@gmail.com (G. Anandha Babu).

1386-1425/$ – see front matter © 2011 Elsevier B.V. All rights reserved.
doi:10.1016/j.saa.2011.08.003

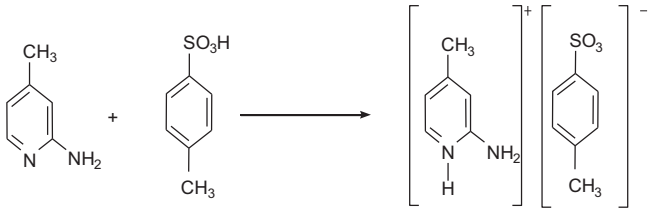

Fig. 1. Reaction of 2 Amino 4-Picoline with p-Toluene sulfonic acid.

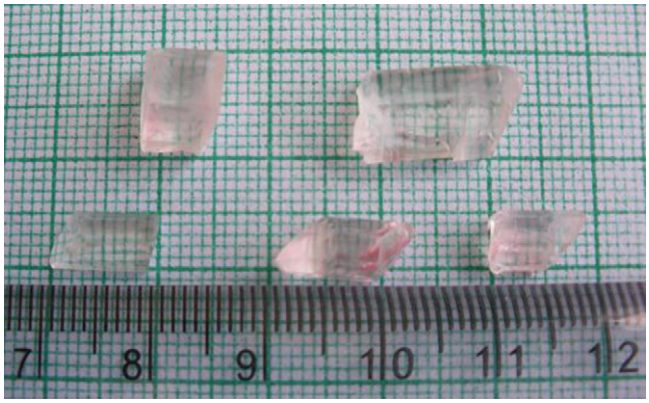

Fig. 2. Grown single crystals of 2A4PTS.

CAD4-MV31 (graphite-monochromated, CuKα = 1.54180 Å). The crystal structure was solved by a direct method with the SIR97 [11] program and refined by full matrix least-squares with SHELX97 [12] program to an *R* value of 0.0544. The structure was solved by direct methods and full-matrix least-squares refinements were performed on F^2 using all unique reflections. All nonhydrogen atoms were refined with anisotropic atomic displacement parameters and the hydrogen atoms were refined with isotropic displacement factors. Drawings of the molecular structure (Fig. 3) and the packing diagram (Fig. 4) were obtained using PLATON. Further crystal data, experimental conditions and structural refinement parameters are presented in Table 1. The crystallographic information file has been deposited by us in the Cambridge structure database (CCDC 781115).

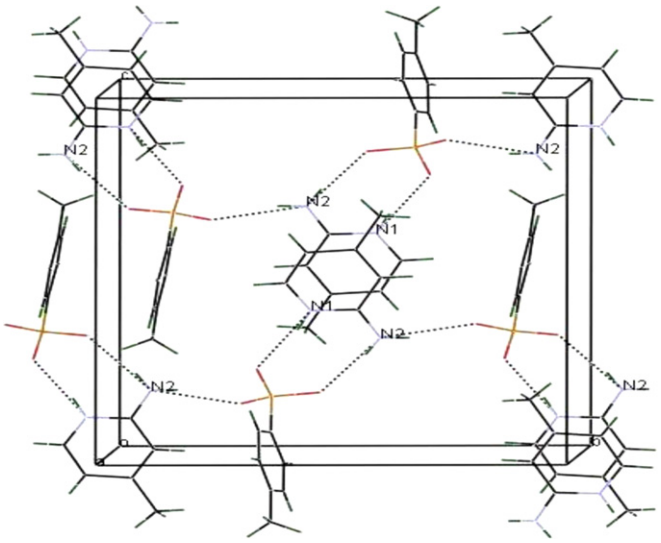

Fig. 4. Packing diagram of 2A4PTS.

2A4PTS crystallizes in the centrosymmetric space group $P2_1/c$ with four formula units of $C_6H_7N_2^+ \cdot C_7H_7SO_3^-$ in the unit cell. A formula unit consists of one 2-amino-4-picolinium cation and one toluene sulfonate anion as shown in Fig. 3.

The protonated N1 atom has lead to a slight increase in the C5–N1–C1 angle to 122.2(2)°. The bond lengths and angles are normal [13]. In the crystal packing (Fig. 4), the protonated N1 atom and 2-amino group (N2) are hydrogen-bonded to the sulfonate oxygen atoms (O2, O3 and O4) via a pair of N–H···O hydrogen bonds and protonated N1 atom is hydrogen bonded sulfonate sulfur atom via a N–H···S hydrogen bond. The crystal structure is stabilized by intramolecular hydrogen bonds to form a three-dimensional network. It should be mentioned that hydrogen bonds are a kind of NLO functional bonds in the crystallographic frame, which was first highlighted by Xue et al. [14–17].

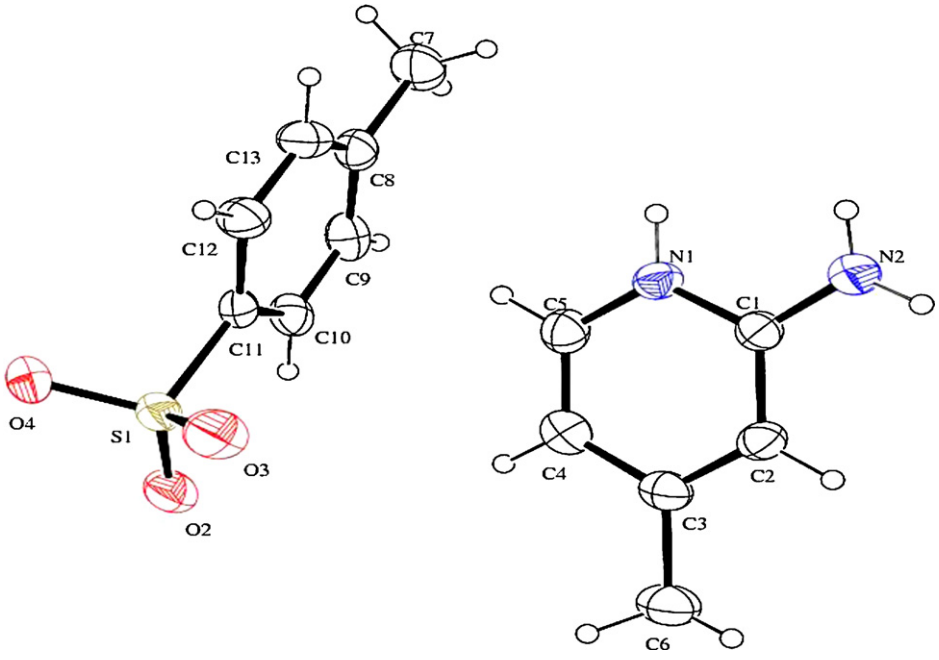

Fig. 3. ORTEP diagram of 2A4PTS.

Table 1
Crystal data and structure refinement of 2A4PTS.

Empirical f ormula	$C_{13}H_{16}N_2O_3S$
Formula weight	280.34
Temperature	293(2) K
Wavelength	1.54180 Å
Crystal system	Monoclinic
Space group	$P2_1/c$
Unit cell dimensions	$a = 7.2442(8)$ Å, $\alpha = 90°$
	$b = 13.359(3)$ Å, $\beta = 98.152(13)°$
	$c = 14.655(3)$ Å, $\gamma = 90°$
Volume	1404.0(4) Å^3
Z	4
Calculated density	1.326 g/cm^3
Absorption coefficient	2.110 mm^{-1}
F(0 0 0)	592
Crystal size	0.30 × 0.20 × 0.20 mm^3
Theta range for data collection	4.50–65.14°
Limiting indices	$-8 \le h \le 8$, $0 \le k \le 15$, $-17 \le l \le 0$
Reflections collected/unique	2499/2399 [R(int) = 0.0365]
Completeness to theta	65.14, 99.8%
Absorption correction	Psi-scan
Max. and min. transmission	0.7882 and 0.6511
Refinement method	Full-matrix least-squares on F^2
Data/restraints/parameters	2399/0/190
Goodness-of-fit on F^2	1.084
Final R indices [$I > 2$sigma(I)]	$R1 = 0.0514$, $wR2 = 0.1365$
R indices (all data)	$R1 = 0.0613$, $wR2 = 0.1446$
Extinction coefficient	0.0206(15)
Largest diff. peak and hole	0.384 and −0.307 e/Å^3

3.2. Multicrystal X-ray diffractometry

The crystalline perfection of the grown single crystals was characterized by HRXRD by employing a multicrystal X-ray diffractometer developed at NPL [18]. The well-collimated and monochromated MoKα_1 beam obtained from the three monochromator Si crystals set in dispersive (+, −, −) configuration has been used as the exploring X-ray beam. The specimen crystal is aligned in the (+, −, −, +) configuration. Due to dispersive configuration, though the lattice constant of the monochromator crystal(s) and the specimen are different, the unwanted dispersion broadening in the diffraction curve (DC) of the specimen crystal is insignificant. The specimen can be rotated about the vertical axis, which is perpendicular to the plane of diffraction, with minimum angular interval of 0.4″. The rocking or diffraction curves were recorded by changing the glancing angle (angle between the incident X-ray beam and the surface of the specimen) around the Bragg diffraction peak position θ_B (taken as zero for the sake of convenience) starting from a suitable arbitrary glancing angle and ending at a glancing angle after the peak so that all the meaningful scattered intensities on both sides of the peak are included in the diffraction curve. The DC was recorded by the so-called ω scan wherein the detector was kept at the same angular position $2\theta_B$ with wide opening for its slit. This arrangement is very appropriate to record the short range order scattering caused by the defects or by the scattering from local Bragg diffractions from agglomerated point defects or due to low angle and very low angle structural grain boundaries [19].

Before recording the diffraction curve to remove the non-crystallized solute atoms which remained on the surface of the crystal and the possible layers which may sometimes form on the surfaces on crystals grown by solution methods [20] and also to ensure the surface planarity, the specimen was first lapped and chemically etched in a non preferential enchant of water and acetone mixture in 1:2 volume ratio.

Fig. 5 shows the high-resolution diffraction curve (DC) recorded for a typical 2A4PTS crystal grown by SEST method using (2 0 0) diffracting planes. As seen in Fig. 5, the DC contains a single peak and indicates that the specimen is free from structural grain boundaries. The FWHM (full width at half maximum) of the curve is 34″ which

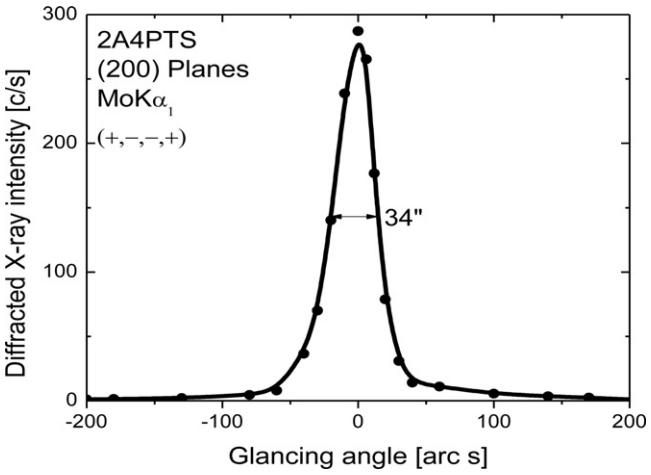

Fig. 5. High-resolution X-ray diffraction curve recorded for a typical 2A4PTS single crystal specimen using (2 0 0) diffracting planes.

is somewhat more than that expected from the plane wave theory of dynamical X-ray diffraction [21], for an ideally perfect crystal but close to that expected for nearly perfect real life crystals. This much broadness with good scattered intensity along both the wings of the DC indicates that the crystal contains both vacancy and interstitial type of defects [22]. More details may be obtained from the study of high-resolution diffuse X-ray scattering measurements [23], which is not the main focus of the present investigation.

3.3. Fourier transform spectral analysis

The FTIR spectrum was recorded using Perkin Elmer FTIR spectrophotometer (KBr pellet technique) in the range 4000–450 cm^{-1}. The recorded FTIR spectrum of 2A4PTS is shown in Fig. 6. The aromatic C=N stretching vibration appears as a sharp band at 1677 cm^{-1}. As expected the asymmetric deformation mode of sulfonyl groups appears at 1385 cm^{-1} and the corresponding symmetric mode exhibits a band at 1176 cm^{-1}. The aromatic C=C stretching vibration brings forth a sharp band at 1486 cm^{-1}. The aromatic C–H in plane bending modes are at 1033 cm^{-1} and 1008 cm^{-1}. The observed wave numbers and the assignments made from the recorded spectra for 2A4PTS crystal are given in Table 2.

3.4. UV–visible spectral analysis

The UV–Vis–NIR transmission spectrum of the as grown 2A4PTS crystal has been recorded using a Perkin Elmer UV–Vis–NIR spectrophotometer in the wavelength range 200–1100 nm and is shown

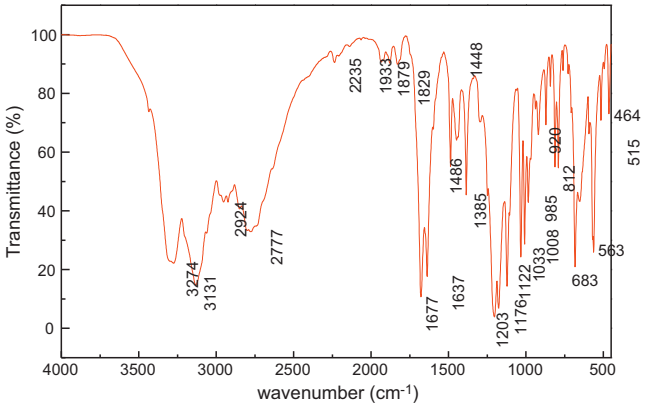

Fig. 6. FTIR spectrum of 2A4PTS.

Table 2
Spectral data and their assignments for 2A4PTS.

FTIR (cm^{-1})	Assignments
3274	$\nu_{as}(NH_2)$
3131	$\nu(NH^+)$
2924	ν(C–H)
2777	ν(C–H) of CH_3 group
1677	ν(C=N)
1486	ν(C=C)
1385	$\nu_{as}(SO_3)$
1176	$\nu_s(SO_3)$
1637	$\delta_{in\ plane}$(N–H)
1033	$\delta_{in\ plane}$(C–H)
1008	$\delta_{in\ plane}$(C–H)
812	$\delta_{out\ plane}$(C–H)
683	$\delta_{out\ plane}$(N–H)

in Fig. 7. From the spectrum, it is noted that the UV transparency cutoff occurs at 350 nm, and there is no remarkable absorption in the entire region of the spectra. The transmittance of 2A4PTS is 30–40%, which is good enough for the generation of higher harmonic light using infrared lasers through NLO phenomena. Since the crystal is transparent in the region 350–1100 nm, one can use 2A4PTS as third harmonic generator of Nd:YAG (λ = 1064 nm) laser to produce ~354.6 nm.

3.5. Thermal analysis

Thermal analysis for 2A4PTS was taken using SDT Q 600 system. The TG results reveal no weight loss below 200 °C and hence the crystal is found to be free from physically absorbed lattice-entrapped water. There is a major weight loss close to 250 °C resulting in the decomposition of the compounds of the crystal. The TG/DTA curves of 2A4PTS are shown in Fig. 8. Fig. 8 shows that there is a sharp endothermic reaction with the maximum temperature at 133 °C which is assigned to the melting of the crystal.

3.6. Laser damage threshold measurement

A Q-switched Nd:YAG Innolas laser of pulse width 7 ns and 10 Hz repetition rate operating in TEM_{00} mode is used as the source. The energy per pulse of 532 nm laser radiation attenuated using appropriate neutral density filters is measured using an energy meter (Coherent EPM 200) which is externally triggered by the Nd:YAG laser. For both single and multiple shot experiments, the sample is mounted on an *X–Y* translator which facilitates in bringing different areas of the sample for exposure precisely. For surface damage, the sample is placed at the focus of a plano-convex lens of focal length 80 mm. The sample is placed 1 cm away from the focus. The onset of damage can be determined by visual damage and audible cracking.

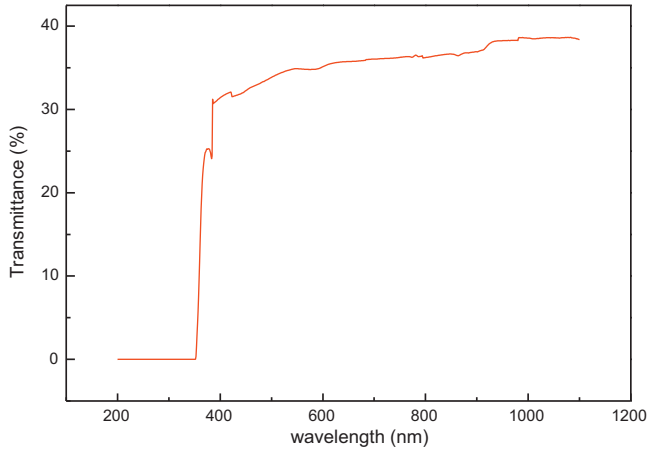

Fig. 7. UV–Vis spectrum of 2A4PTS.

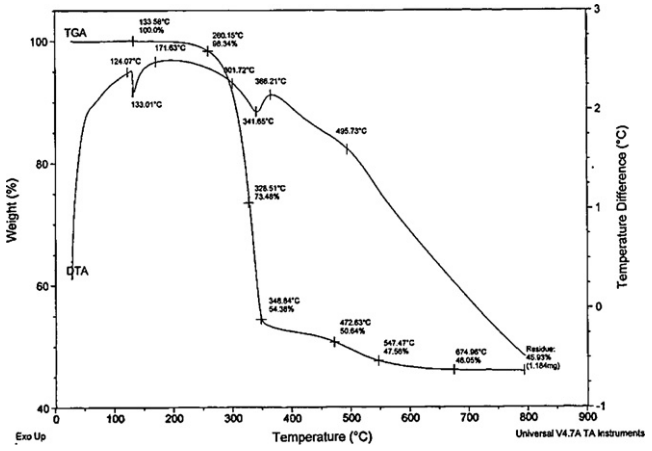

Fig. 8. TG–DTA curves of 2A4PTS.

The utility of NLO crystal depends not only on the linear and nonlinear optical properties but also largely on its ability to withstand high power lasers. The bulk materials appear more damage-resistant than the surfaces. The damage threshold depends on a great number of laser parameters such as wavelength, energy, pulse duration, transverse and longitudinal mode structure, beam size, location of beam etc. The diameter of the focused spot is calculated to be 1.08 mm using knife edge method. Single shot and multiple shot (150 pulses) surface laser damage thresholds are determined to be 0.55 GW/cm^2 and 0.36 GW/cm^2, respectively, at 532 nm laser radiation.

The damage pattern of 2A4PTS shows tiny circular blobs surrounding the core of the damage. Such circular blobs are generally seen in crystals where the damage is mainly due to thermal effects resulting in melting and solidification or decomposition of the material. It is most likely that in the present case damage occurs due to decomposition of the crystal. Hence, in 2A4PTS we can expect the damage to be of thermal origin. However, one cannot rule out other mechanisms being operative simultaneously, as the damage mechanism is quite complex and depends on the nature of the material and various experimental parameters.

3.7. Z-scan measurements

The third-order nonlinear refractive index n_2 and the nonlinear absorption coefficient β of aqueous solution of the 2A4PTS was evaluated by the Z-scan technique. A diode-pumped Nd:YAG (Coherent Compass TM 215M-50) laser of wavelength 532 nm was used as source. The Gaussian profile laser beam was focused on a 1 mm cuvette containing the 1 mM concentration solution by lens of focal length 3.5 cm to produce a beam waist ω_o of 15.84 μm. The sample is translated from −10 mm to 10 mm with $Z = 0$ at the focus of the lens in order to vary the incident intensity falling on the sample and the corresponding output transmittance was measured. The transmission of the beam through an aperture placed in the far field was measured using a photo detector fed to the digital power meter. For the open aperture Z-scan, a lens to collect the entire laser beam transmitted through the sample replaced the aperture.

$|\Delta\varphi_o|$, the on-axis phase shift at the focus is related to the difference in the peak and valley transmission, $|Tp–v|$, as

$$\Delta T_{p-v} = 0.406(1-S)^{0.25}|\Delta\varphi_o| \quad (1)$$

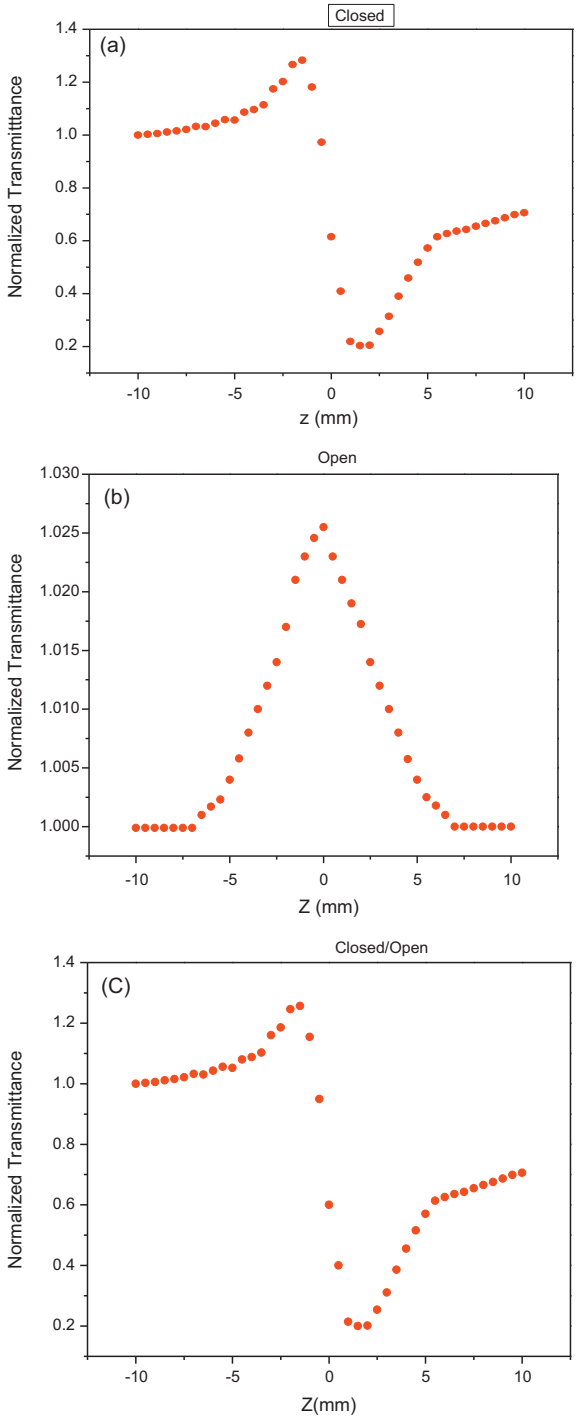

Fig. 9. (a) Closed aperture scan; (b) open-aperture scan; and (c) the division of (a) by (b).

where $S = 1 - \exp(-2r_o^2/\omega_o^2)$ is the aperture linear transmittance with r_o denoting the aperture radius and ω_o denoting the beam radius at the aperture in the linear regime. Then nonlinear refractive index is given by

$$n_2 = \frac{\Delta\varphi_o\lambda}{2\pi I_o L_{eff}} \quad (2)$$

where λ is the laser wavelength, I_o is the intensity of the laser beam at focus $Z = 0$, $L_{eff} = [1 - \exp(-\alpha L)/\alpha]$ is the effective thickness of the sample, α is the linear absorption coefficient and L is the thickness of the sample. Generally the measurements of the normalized transmittance versus sample position, for the cases of closed and open aperture, allow determination of the nonlinear refractive index, n_2, and the saturation absorption coefficient, β. Here, since the closed-aperture transmittance is affected by the nonlinear refraction and absorption, the determination of n_2 is less straight forward from the closed-aperture scans. It is necessary to separate the effect of nonlinear refraction from that of the nonlinear absorption. A method to obtain purely effective n_2 is to divide the closed-aperture transmittance by the corresponding open-aperture scans. The ratio of Fig. 9(a) and (b) scans is shown in Fig. 9(c). The data obtained in this way reflects purely the effects of nonlinear refraction.

Table 3
Nonlinear optical parameters.

Sample	$n_2 \times 10^{-8}$ cm^2/W	$\beta \times 10^{-4}$ cm/W	$\chi^{(3)} \times 10^{-6}$ esu
2A4PTS	−6.8	−7.7	3.38

The nonlinear absorption coefficient β can be estimated from the open-aperture Z-scan data.

$$\beta = \frac{2\sqrt{2}\Delta T}{I_o L_{eff}} \quad (3)$$

The nonlinear refraction index coefficient, n_2, the nonlinear absorption coefficient, β, and susceptibility, $\chi^{(3)}$, for solution of 2A4PTS in water using the Z-scan technique with 532 nm diode pumped Nd:YAG laser is given in Table 3. The Z-scan measurements indicate that the 2A4PTS exhibits negative nonlinear optical properties. It is shown that the nonlinear absorption can be attributed to a saturation absorption process, while the nonlinear refraction leads to self-defocusing in the compound.

3.8. Mechanical hardness

The structure and composition of the crystalline solids are inviolably related to the mechanical hardness [24–26]. The Vickers hardness is one of the important deciding factors in selecting the processing (cutting, grinding and polishing) steps of bulk crystal in the fabrication of devices based on the crystals. It is, therefore, important to study the mechanical properties of organic NLO crystals.

Vickers microhardness measurement studies were also carried out using a MITUTOYO model HM112 hardness tester. Microhardness testing is one of the best methods of understanding the mechanical properties of materials such as hardness number, crack length, fracture toughness, brittle index, and elastic stiffness constant. Hardness of a material is a measure of resistance it offers to local deformation [27]. The hardness measurements were made on

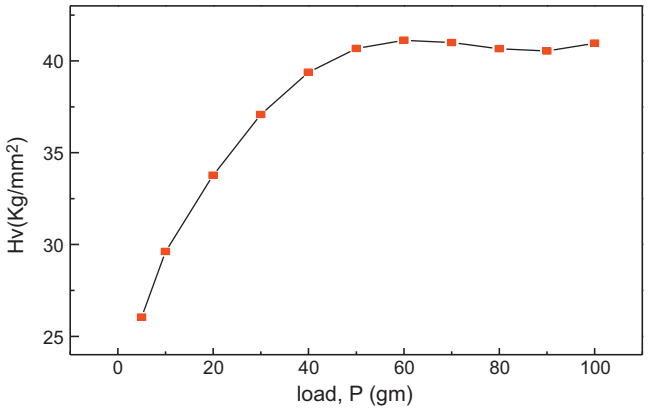

Fig. 10. Mechanical behavior of 2A4PTS: load versus hardness number.

2A4PTS crystal. Loads ranging from 5 to 100 g were used for making indentations, keeping the time of indentation constant at 10 s for all the cases. The diagonal lengths of the indentation mark and crack length were measured, using the micrometer eyepiece. The microhardness value was calculated using

$$H_v = \frac{1.8544P}{d^2}\ \mathrm{kg/mm^2}$$

where H_v is the Vickers hardness number, P is the applied load and d is the diagonal length of the indentation. Fig. 10 shows the variation of H_v as a function of applied load ranging from 5 g to 100 g on 2A4PTS crystal. It is very clear from the figure that H_v increases with the increase of load and then is saturated.

4. Conclusion

Single crystals of 2A4PTS were grown using solution growth technique. The crystal structure of 2A4PTS was determined by single crystal X-ray diffraction analysis. The high resolution X-ray diffraction curve (DC) measurements substantiate the good quality of the crystals. The functional group was confirmed by FTIR. Optical transmittance window and the lower cutoff wavelength have been identified through UV–Vis–NIR spectrum. The thermal behavior of the grown crystals was studied using TG-DTA. Single shot and multiple shot (50 pulses) surface laser damage thresholds are determined to be 0.55 GW/cm^2 and 0.36 GW/cm^2 at 532 nm laser radiation, respectively.

From the mechanical measurements, it was observed that the hardness increases with increase of load and then is saturated. The NLO test was carried out by Z-scan technique and affirms that 2A4PTS exhibits the nonlinear optical properties.

Acknowledgment

We thank Dr. G. Bhagavannarayana, National Physical Laboratory, New Delhi for HRXRD studies.

References

[1] D.F. Eaton, Science 25 (1991) 281.
[2] P.N. Prasad, D.J. Williams, Introduction to Nonlinear Optical Effects in Organic Molecules and Polymers, Wiley, New York, 1991.
[3] Z. Latajka, G. Gajewski, A.J. Barnes, D. Xue, H. Ratajczak, J. Mol. Struct. 928 (2009) 121.
[4] X. Gu, D. Xue, H. Ratajczak, J. Mol. Struct. 887 (2008) 56.
[5] X. Ren, D. Xu, D. Xue, J. Cryst. Growth 310 (2008) 2005.
[6] D. Xu, D. Xue, J. Cryst. Growth 310 (2008) 1385.
[7] X. Yan, D. Xu, D. Xue, Acta Mater. 55 (2007) 5747.
[8] D. Xu, D. Xue, J. Cryst. Growth 286 (2006) 108.
[9] D. Xue, L. Zou, L. Wang, X. Yan, Mod. Phys. Lett. B 23 (2009) 3761.
[10] D. Xue, X. Yan, L. Wang, Powder Technol. 191 (2009) 98.
[11] A. Altomare, G. Cascarno, A. Guagliardi, A.G.G. Moliterni, M.C. Burla, G. Polidori, M. Camalli, R. Spagna, J. Appl. Crystallogr. 32 (1999) 115–119.
[12] G.M. Sheldrick, SHELX97, Program for the Crystal Structure Refinement, University of Gottingen, Germany, 1997.
[13] F.H. Allen, O. Kennard, D.G. Watson, L. Brammer, A.G. Orpen, R. Taylor, J. Chem. Soc. Perkin Trans. 2 (1987) S1–S19.
[14] D. Xue, S. Zhang, Chem. Phys. Lett. 301 (1999) 449.
[15] D. Xue, H. Ratajczak, J. Mol. Struct. (Theochem) 716 (2005) 207.
[16] D. Xue, S. Zhang, J. Solid State Chem. 135 (1998) 121.
[17] F. Zhang, D. Xue, Mod. Phys. Lett. B 23 (2009) 3943.
[18] K. Lal, G. Bhagavannarayana, J. Appl. Crystallogr. 22 (1989) 209.
[19] G. Bhagavannarayana, S.K. Kushwaha, J. Appl. Crystallogr. 43 (2010) 154.
[20] G. Bhagavannarayana, S. Parthiban, S. Meenakshisundaram, J. Appl. Crystallogr. 39 (2006) 784.
[21] B.W. Batterman, H. Cole, Rev. Mod. Phys. 36 (1964) 681.
[22] G. Bhagavannarayana, S. Parthiban, S. Meenakshisundaram, Cryst. Growth Des. 8 (2008) 446–451.
[23] K. Lal, G. Bhagavannarayana, J. Appl. Crystallogr. 22 (1989) 209–215.
[24] K. Li, D. Xue, Phys. Scr. T139 (2010) 014073.
[25] K. Li, D. Xue, Chin. Sci. Bull. 54 (2009) 131.
[26] K. Li, X. Wang, F. Zhang, D. Xue, Phys. Rev. Lett. 100 (2008) 235504.
[27] W. Mott, Micro Indentation Hardness Testing, Butterworths, London, 1956.